scientific reports

Check for updates

OPEN

Functional pathogenicity of *ESRRB* variant of uncertain significance contributes to hearing loss (DFNB35)

Won Hoon Choi[1,6], Yeijean Cho[2,6], Ju Hyuen Cha[1], Dae Hee Lee[3], Jong Gwan Jeong[3], Sung Ho Jung[1], Jae-Jin Song[1], Jun Ho Lee[1] & Sang-Yeon Lee[1,4,5]✉

Advances in next-generation sequencing technologies have led to elucidation of sensorineural hearing loss genetics and associated clinical impacts. However, studies on the functional pathogenicity of variants of uncertain significance (VUS), despite their close association with clinical phenotypes, are lacking. Here we identified compound heterozygous variants in *ESRRB* transcription factor gene linked to DFNB35, specifically a novel splicing variant (NM_004452.4(ESRRB): c.397 + 2T>G) *in trans* with a missense variant (NM_004452.4(ESRRB): c.1144C>T p.(Arg382Cys)) whose pathogenicity remains unclear. The splicing variant (c.397 + 2T>G) caused exon 4 skipping, leading to premature stop codon formation and nonsense-mediated decay. The p.(Arg382Cys) variant was classified as a VUS due to its particularly higher allele frequency among East Asian population despite disease-causing in-silico predictions. However, functional assays showed that p.(Arg382Cys) variant disrupted key intramolecular interactions, leading to protein instability. This variant also reduced transcriptional activity and altered expression of downstream target genes essential for inner ear function, suggesting genetic contribution to disease phenotype. This study expanded the phenotypic and genotypic spectrum of *ESRRB* in DFNB35 and revealed molecular mechanisms underlying *ESRRB*-associated DFNB35. These findings suggest that variants with high allele frequencies can also possess functional pathogenicity, providing a breakthrough for cases where VUS, previously unexplored, could be reinterpreted by elucidating their functional roles and disease-causing characteristics.

Keywords *ESRRB*, DFNB35, Variant of uncertain significance, Functional study, Allele frequency

Sensorineural hearing loss (SNHL), a condition marked by impaired sound signaling in the auditory sensory system, is the most prevalent sensory deficit. Since the 2010s, the genetic architecture of SNHL has been extensively elucidated[1], particularly in monogenic forms of deafness, due to advancements in next-generation sequencing (NGS) technologies. In parallel with this, mouse genetics studies have helped reveal the physiological basis of SNHL in humans and associated molecular functions[2]. Over 150 causative genes have been implicated in SNHL, with diagnostic yields ranging from 12.7% to 64.3% by targeted sequencing[3–6]. It is known that complete genetic diagnosis provides additional benefits in clinical practice, including targeted agents[7,8], referral to specialists[9], individualized auditory rehabilitation[10], and reproductive consultation[11]. However, the process of identifying causative variants of SNHL remains complex due to genetic and phenotypic heterogeneity[12]. In addition, the spectrum of deafness-causing genetic variants differs greatly among geographical areas and ethnicities[13]. In response to this challenge, a framework of hearing loss genes based on molecular mechanisms of inner-ear function has emerged[1], including (1) hair bundle development and functioning; (2) synaptic transmission; (3) cellular adhesion and maintenance; (4) cochlear ion homeostasis; (5) extracellular matrix; (6) oxidative stress, metabolism, and mitochondrial defects; and (7) transcriptional regulation.

[1]Department of Otorhinolaryngology-Head and Neck Surgery, Seoul National University Hospital, Seoul National University College of Medicine, Seoul, Republic of Korea. [2]Seoul National University College of Medicine, Seoul, South Korea. [3]CTCELLS, Inc., 21, Yuseong-Daero, 1205 Beon-Gil, Yuseong-Gu, Daejeon, Republic of Korea. [4]Sensory Organ Research Institute, Seoul National University Medical Research Center, Seoul, Republic of Korea. [5]Department of Genomic Medicine, Seoul National University Hospital, Seoul National University College of Medicine, Seoul, Republic of Korea. [6]These authors contributed equally: Won Hoon Choi and Yeijean Cho. ✉email: maru4843@hanmail.net

Biallelic variants of *ESRRB,* a transcriptional factor gene, have been associated with autosomal recessive hearing loss (DFNB35). *ESRRB* is located at the 14q24.3 locus. It encodes a steroid hormone receptor known as estrogen-related receptor beta (ERR beta), a member of the nuclear receptor family[14]. Although the structure of ERR beta has been established[15], the exact mechanism involved in its response to estrogens and specific physiological ligands that bind to ERR beta remains poorly understood. *ESRRB* serves as a transcriptional factor that can regulate transcriptional activities of target genes including *GATA6*, *NR0B1*, *Pou5F1*, and *PERM1*[16]. To date, less than 20 families with SNHL exclusively of Pakistani ethnicity have been diagnosed with *ESRRB* biallelic variants presumably due to disruptions in transcriptional regulation and post-transcriptional modifications[1]. However, limited dataset precludes the development of genotype–phenotype correlations and functional characterizations of disease-causing variants, necessitating additional evidence.

Herein, we report the first case harboring *ESRRB* compound heterozygous variants in South Korea, specifically a novel splicing variant (NM_004452.4(ESRRB): c.397 + 2T>G) *in trans* with a missense variant (NM_004452.4(ESRRB): c.1144C>T p.(Arg382Cys)) underlying *ESRRB*-associated DFNB35. The missense variant, p.(Arg382Cys), has been a recurring mutant allele in the literature[17–19]. However, the pathogenicity of this allele remains questionable. Notably, the allele frequency of this variant was found to be much higher in East Asians, especially in Korean population, resulting in its pathogenicity classification as a variant of uncertain significance (VUS) according to ACMG-AMP guideline[20]. Recently, ACGS Best Practice Guidelines for Variant Classification in Rare Disease recommend reporting a VUS with a high level of supporting evidence, such as 'hot/warm VUS'. Approaches that secure evidence for the pathogenicity of VUS through functional analysis aim to uplift the classification of these VUS to 'likely pathogenic' or 'pathogenic'[21].

Through molecular modeling, dynamics, and functional assays, this study for the first time reveals functional pathogenicity of the outlier variant p.(Arg382Cys). This breakthrough extends our current understanding of SNHL genetics, particularly by elucidating functional roles and disease-contributing characteristics of VUS. Our study challenges traditional views on the correlation between allele frequency and pathogenicity, proposing that VUS, a previously underestimated variant, could be reinterpreted as critical in disease caution. This revelation could potentially broaden the scope of genetic factors implicated in the development of SNHL.

Results

Clinical phenotype and genotype

The proband (SNUH635-1252) was a sporadic SNHL case in the SNUH635 family (Fig. 1a). Hearing impairment was congenital or evident at prelingual onset. Audiogram showed asymmetric hearing loss characterized by moderate SNHL in the right ear, contrasted by severe-to-profound SNHL in the left ear (Fig. 1b). Over the course of a 17-year monitoring period, audiograms exhibited a progressive nature of hearing loss in the right ear (Fig. 1b). Neither temporal bone computed tomography (CT) nor internal acoustic canal magnetic resonance imaging (MRI) revealed any anomalies within the inner ear (data not shown). Additionally, tests for congenital cytomegalovirus (cCMV) infections, including CMV culture and viral load via real-time PCR, were normal. A comprehensive evaluation of the proband's medical history and physical examination disclosed no other phenotypes or underlying diseases. Parents displayed normal hearing without any additional disease phenotypes.

Through whole exome sequencing (WES) and bioinformatics analysis, *ESRRB* compound heterozygous variants, specifically a canonical splicing variant (c.397 + 2T>G:p.?) *in trans* and a missense variant (c.1144C>T:p.(Arg382Cys)), were identified in one proband (SNUH635-1252). Co-segregation analysis using Sanger sequencing (Fig. 1c) confirmed that these two variants, c.397 + 2T>G and c.1144C>T, were inherited from paternal and maternal alleles, respectively. In the analysis of copy number variations (CNVs) through CNVkit and copy number inference from exome reads (CoNIFER) algorithms, no occurrences of causative deletions or duplications were identified in exomes of the proband with respect to 745 genes linked to hearing loss (Table S1). In addition, copy number changes in *ESRRB* coding genomic regions were not depicted in the Integrative Genomics Viewer (IGV).

Splicing impact of c.397 + 2T>G

To investigate the impact of the *ESRRB* c.397 + 2T>G variant on splicing, both wild-type and mutant *ESRRB* minigenes encompassing exon 4 and adjacent intronic regions were generated (Fig. 2a). To assess differential effects on pre-mRNA splicing, HEK293T cells were transfected with wild-type or *ESRRB* c.397 + 2T>G variant minigenes. Minigene assay results indicated contrasting electrophoretic profiles for the wild-type and the c.397 + 2T>G mutant *ESRRB* minigenes when they were transfected into HEK293T cells (Fig. 2b). Specifically, the wild-type minigene yielded a single, identifiable band of 670 bp, while the mutant variant exhibited one distinct band of 260 bp consistent with skipping of exon 4. Sanger sequencing results showed that the larger fragment contained *ESRRB* exon 4 flanked by two exons of the pSPL3 vector (exon A and exon B), while the smaller one contained only pSPL3 exons (Fig. 2c). In alignment with bioinformatics analysis, the c.397 + 2T>G splicing event was observed to induce exon 4 skipping, leading to formation of a premature stop codon followed by nonsense-mediated decay (NMD). This process is implicated in pathogenicity.

Allele frequency and in-silico prediction of p.Arg382Cys

The missense variant, p.(Arg382Cys), is located in the Ligand-Binding Domain (LBD), which serves as transcriptional regulators of estrogen target genes[14]. The amino acid residue at position Arg382 exhibits high conservation across orthologous genes in multiple species (Fig. 1d), further supporting its potential functional significance. The variant p.(Arg382Cys) also displayed substantial in silico impact via Combined Annotation Dependent Depletion (CADD) phred and Rare Exome Variant Ensemble Learner (REVEL) algorithms, scoring 25.1 and 0.709, respectively. However, the allele frequency of c.1144C>T: p.(Arg382Cys) variant was relatively

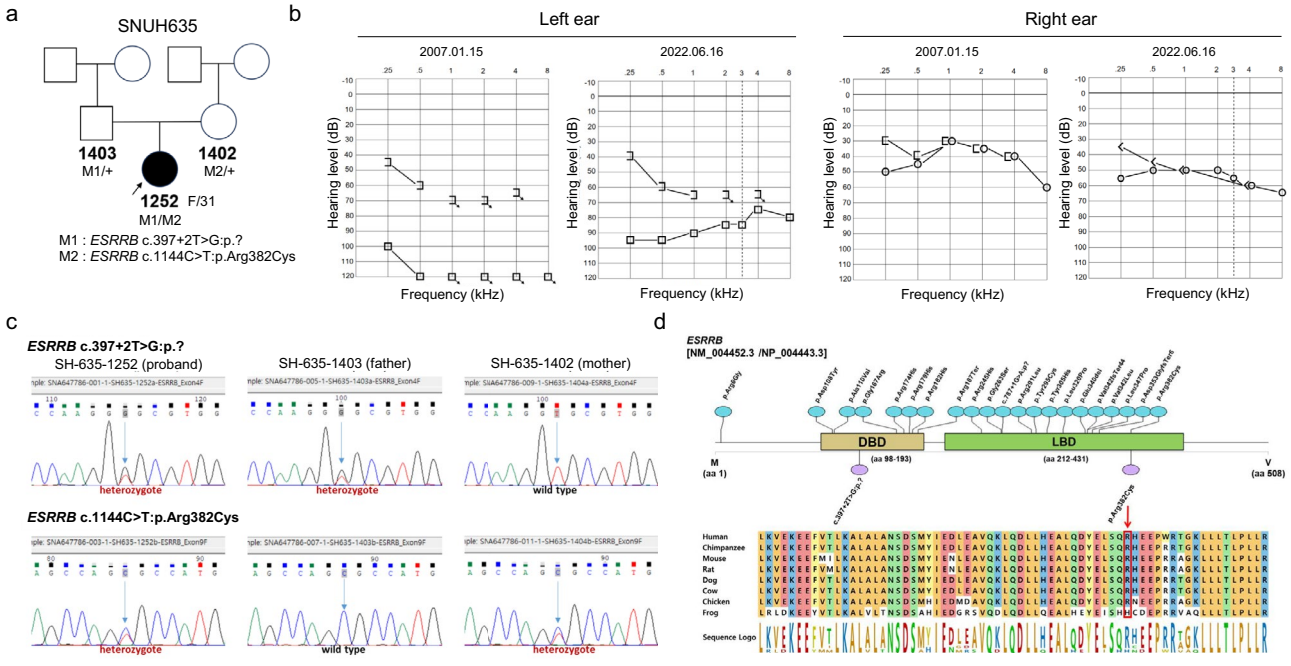

Fig. 1. Phenotypic and genotypic characterization of *ESRRB* compound heterozygous variants. (**a**) Pedigree of a Korean family (SNUH635) harboring *ESRRB* compound heterozygous variants, specifically a novel splicing variant (c.397 + 2T>G:p.?) *in trans* with a missense variant (c.1144C>T:p.(Arg382Cys)). Filled symbols and opened symbols indicate affected and unaffected individuals, respectively. (**b**) Audiograms reveal an asymmetrical sensorineural hearing loss, characterized as moderate in the right ear and severe-to-profound in the left ear. Sequential audiograms spanning 17 years, each divided by ear, with the most recent one displayed on the right and the initial one on the left, indicate a progressive nature of hearing loss in the right ear. (**c**) Sanger sequencing chromatograms of the compound heterozygous variants in the SNUH635 family. The arrow indicates the site of the variant. (**d**) The domain (top) and conservation maps (bottom) display *ESRRB* variants previously identified in the literature (blue circles), alongside the novel splicing variant (c.397 + 2T>G:p.?) in trans with a missense variant (c.1144C>T:p.(Arg382Cys)) from this study (purple circle). Conservation maps were visualized using MegAlign Pro (version 17.6). The residue of the p.(Arg382Cys) variant is highly conserved across *ESRRB* orthologs in different species, as highlighted by the red square.

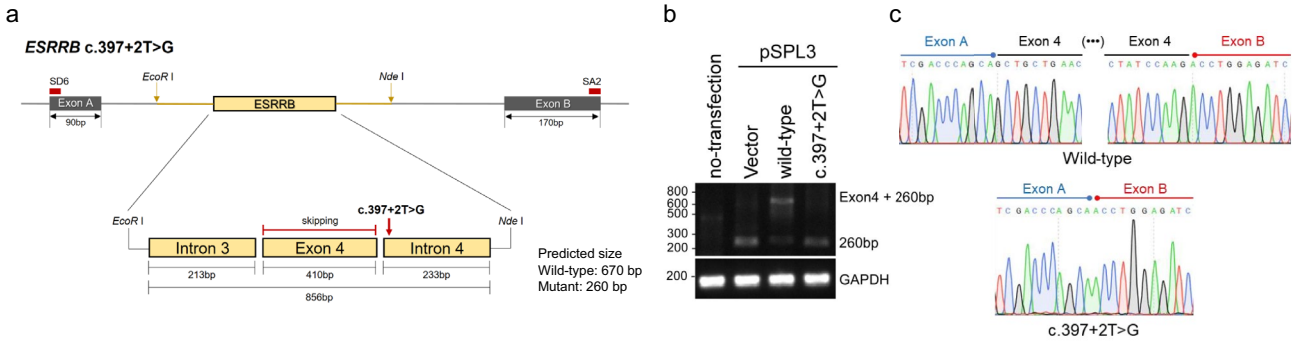

Fig. 2. Impact of the *ESRRB* c.397 + 2T>G variant on splicing. (**a**) A schematic illustration of the pSPL3- *ESRRB* c.397 + 2T>G variant minigenes. Exon 4 of *ESRRB* gene and flanking introns were cloned into EcoRI and NdeI sites of pSPL3 vector featuring either a wild-type or the c.397 + 2T>G variant between two pSPL3 exons (exons A and B). Locations of SD6 and SA2 primers used for splice analysis are also shown. (**b**) HEK293T cells were transfected with either the wild-type or the c.397 + 2T>G variant *ESRRB* minigene, or an empty pSPL3 vector. After RNA extraction and cDNA synthesis, PCR was performed to amplify splicing products using SD6 and SA2 vector-specific primers, which were then analyzed through agarose gel electrophoresis. The wild-type *ESRRB* minigene splice resulted in a 670 bp product. In contrast, the c.397 + 2T>G variant *ESRRB* minigene led to exon skipping and resulted in a 260 bp product. (**c**) Same as in (**b**) except that Sanger sequencing confirmed occurrence of exon4 skipping with c.397 + 2T>G variant *ESRRB* minigene.

high with a score of 0.084 in Korean Variant Archive for a reference database of genetic variations in the Korean population (KOVA2) (Table S2). Additionally, we observed a much higher frequency of this mutant allele predominantly in Korean and East Asian populations compared to other ethnic groups. In detail, the allele frequency of p.(Arg382Cys) variant is 0.007065 among East Asian while the allele frequency among all ethnicities is 0.002095, according to the Genome Aggregation Database (gnomAD) v.4.1.0 (Table S2). At this stage, based on the ACMG-AMP guideline, the p.(Arg382Cys) variant was classified as VUS, evidenced by PM3, PP3, and BA1 due to its trans position with a pathogenic variant, high REVEL score (≥ 0.7), and high allele frequency (≥ 0.005).

Nonetheless, the p.(Arg382Cys) variant is situated in the LBD at the C-terminus of the ESRRB protein, a region known for mutational clustering and essential for maintaining structural stability and transcriptional regulation[14]. Furthermore, the p.(Arg382Cys) variant has been previously identified in patients with SNHL[17–19], albeit with limited functional characterization (Table S3). Given this, its current classification as VUS remains to be investigated for elucidating its pathogenicity through structural and functional studies. Resultantly, according to ACMG-AMP and ClinGen guidelines, we obtained additional evidence of PS3_supporting based on functional assays, thus permitting the reclassification of p.(Arg382Cys) variant as a 'warm VUS.'

Functional characterization of p.Arg382Cys: molecular modeling and dynamics

The crystal structure of the wild-type ESRRB model shows that Arg382 in the wild-type protein can interact with neighboring residues (Lys335, Glu337, and Glu385) through intramolecular interactions (Fig. 3a), including hydrogen bonds and salt bridges, thereby maintaining the structural integrity. However, when Arg382 is substituted with Cys382, these intramolecular interactions with Lys335, Glu337, and Glu385 all collapse, leading to a loss of structural stability (Fig. 3a). Interestingly, the p.(Arg382His) variant, which only retained the Glu337-Arg382His interaction in the 6LIT model (Fig. 3b), did not affect the secondary structure of the surrounding helices containing Glu385 and Lys335, which remained largely unchanged (Fig. 3c). These observations suggest that the interaction between Glu337 and Arg382 would be critical for maintaining the stability of the loop containing Arg382.

To further understand conformational changes in the ESRRB with the p.(Arg382Cys) variant, a molecular dynamics simulation (MDS) was conducted for 100 ns. Several parameters were analyzed throughout the simulation trajectory, including root mean square deviation (RMSD) analysis, root mean square fluctuation (RMSF) analysis, and solvent accessible surface area (SASA). RMSD analysis showed a slightly elevated deviation for the p.(Arg382Cys) variant compared to wild-type counterparts (Fig. 3d). Furthermore, RMSF analysis revealed a significant surge in molecular fluctuation specifically at the Arg382 position due to loss of neighboring interactions notably with Glu337 (Fig. 3e). These observations aligned with a notable expansion in the SASA observed throughout the entire simulation process, diverging significantly from the wild-type ESRRB molecule (Fig. 3f). Indeed, the mutant protein demonstrated a distinctly different pattern of deviation throughout the simulation, while the wild-type protein appeared to be stable (Movie S1). Conversely, no significant alterations in radius of gyration (Rg) were observed between wild-type and mutant protein (Fig. 3g). All these findings support the idea that the p.(Arg382Cys) variant can weaken the loop stability, consequently compromising the overall stability of the ESRRB protein.

Functional characterization of p.Arg382Cys: structure stability and subcellular localization

Molecular modeling and dynamics indicated that p.(Arg382Cys) variant resided in LBD might be potentially involved in protein instability. To determine whether the p.(Arg382Cys) variant could destabilize the encoded protein, we performed CHX chase assays using both HEI-OC1 and HEK293T cells (Figs. 4a and S1A). Consistent with molecular modeling and dynamics studies, the stability of the *ESRRB* p.(Arg382Cys) variant was significantly reduced compared to that of the wild-type (in 8 h, there was a change of 2.37 folds with HEI-OC1 cells and 2.45 folds with HEK293T cells). However, immunocytochemistry data showed that there was no significant difference in the translocation ability of ESRRB into the nucleus between the mutant and the wild type (Figs. 4b and S1b). Aligned with these observations, a subcellular fractionation assay indicated comparable levels of nuclear-localized ESRRB in both the wild-type and mutant (Figs. 4c and S1c).

Functional characterization of p.Arg382Cys: transcriptional activity

To explore the impact of p.(Arg382Cys) variant on transcriptional activity, we utilized pGL4.12[luc2CP]-SMAD7, an SMAD7 luciferase reporter, in HEI-OC1 and HEK293T cells, alone or in combination with wild-type and p.(Arg382Cys) variant (Figs. 4d and S1d). Transient overexpression of the ESRRB wild-type significantly increased luciferase activity, demonstrating a 2.09-fold increase relative to the internal control in HEI-OC1 cells ($p < 0.01$) and 2.21-fold in HEK293T cells ($p < 0.01$). However, the luciferase activity of ESRRB mutant did not exhibit a significant deviation from the internal control, as evidenced by a 1.19-fold change ($p = 0.3$) in HEI-OC1 cells and 1.24-fold in HEK293T cells ($p = 0.09$). Overall, the *ESRRB* p.(Arg382Cys) variant markedly diminished the transcriptional performance required to regulate downstream target gene expression.

Functional characterization: target gene expression

To evaluate molecular consequences of *ESRRB* variants, we conducted qRT-PCR to uncover alterations of *ESRRB* transcriptional profiles in patient-derived cells. Previous studies have characterized ESRRB as a transcription factor for GATA6[16] and analyzed downstream targets of GATA6[22]. We found that a range of genes were differentially expressed with at least a two-fold change after overexpressing GATA6. We focused on those related to hearing loss and inner ear expression. Based on such criteria, five genes encoding transmembrane proteins (*ATP1B1*[23,24] and *NRP1*[25]), cell adhesion proteins (*SPARC*[26]), and transcription factors (*EGR1*[27] and *TBX3*[28]) were selected for qRT-PCR analysis. Notably, in the proband (SH635-1252) and mother (SH635-1402) harboring the

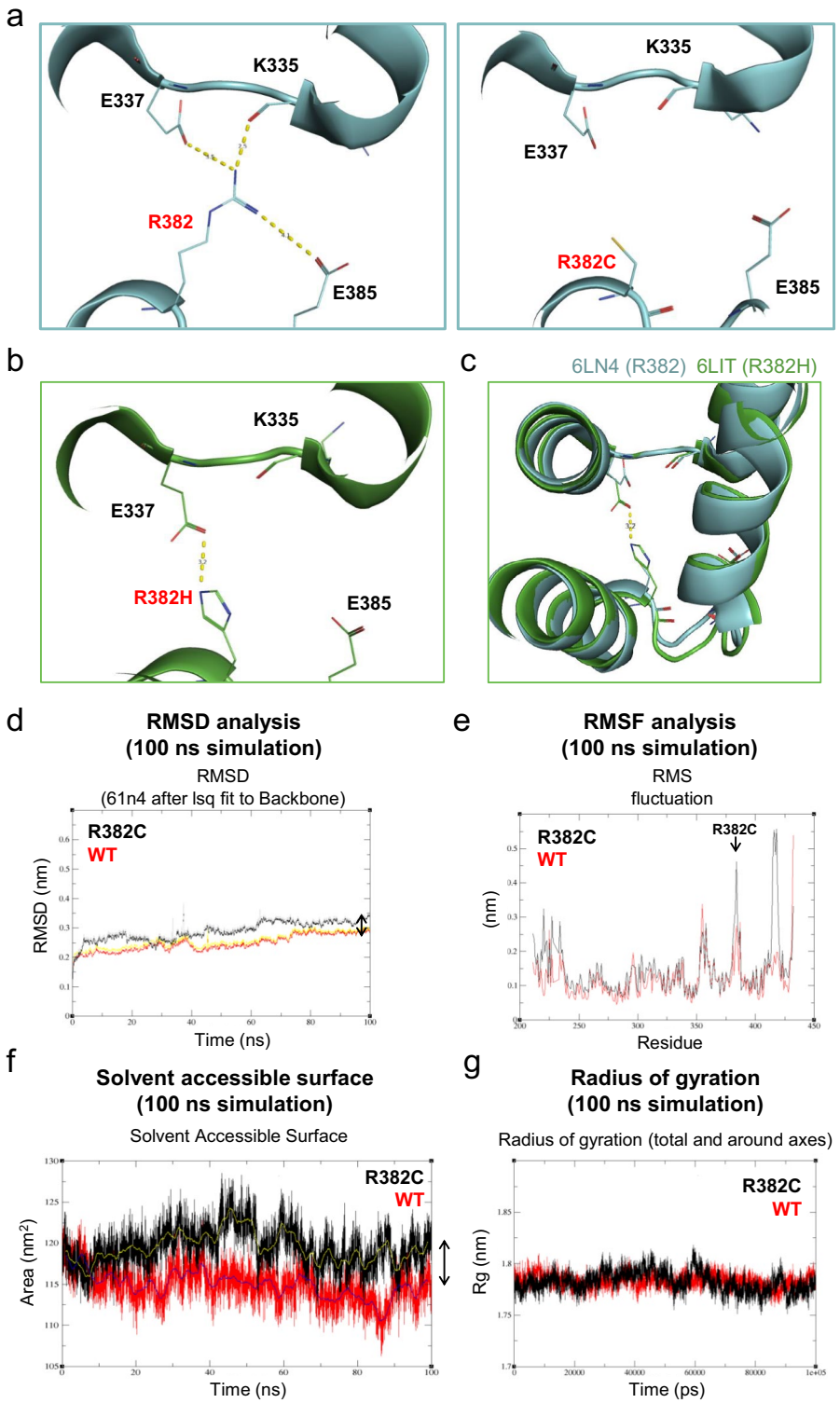

Fig. 3. Effects of *ESRRB* p.(Arg382Cys) variant on molecular structure dynamics. (**a**) Intramolecular interactions of Arg382Cys residue in the wild-type ESRRB (left) and the Arg382Cys mutant (right). Collapsed intramolecular interactions between Cys382, Lys335, Glu337, and Glu385 in the Arg382Cys mutant. (**b**,**c**) Intramolecular interactions of Arg382His mutant (RCSB: 6LIT). Despite the Arg382His mutant retaining interactions solely with Glu337 while losing all other connections with Glu385 and Lys335, the stability and shape of secondary structures containing these residues seems to remain unaffected (**c**). (**d**) Root mean square deviations (RMSDs) of wild-type and Arg382Cys ESRRB. Continuously increased RMSD levels were observed in the Arg382Cys model (red: wild-type (WT), black: Arg382Cys). (**e**) A peak increase (indicated by an arrow) in molecular fluctuation was observed for the Arg382Cys mutant in root mean square fluctuation (RMSF) analysis for 100 ns simulation (red: WT, black: Arg382Cys). (**f**) Increased flexibility of the Arg382Cys containing loop led to a notable expansion in Solvent accessible surface area of ESRRB protein (red: WT, black: Arg382Cys). (**g**) Radius of gyration (Rg) of WT ESRRB (Red) and Arg382Cys ESRRB model. No significant difference in Rg value was observed between WT and Arg382Cys ESRRB.

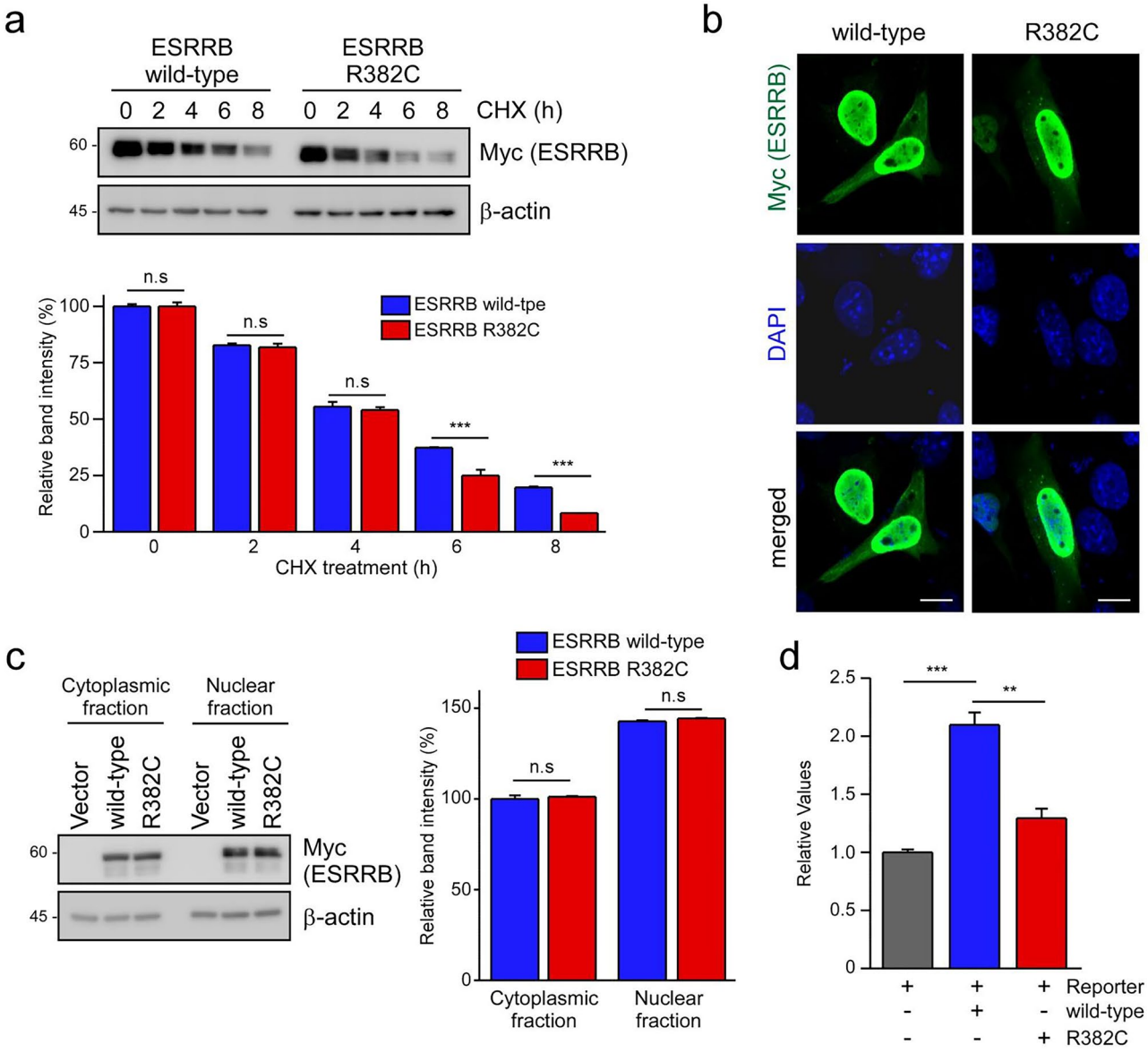

Fig. 4. Effects of *ESRRB* p.Arg382Cys variant on protein stability, subcellular localization and transcriptional activity. (**a**) Wild-type and Arg382Cys mutant ESRRB proteins were transiently overexpressed in HEI-OC1 cell lines. Then cycloheximide (CHX) chase experiments were carried out and whole cell lysates (WCLs) were subjected to SDS-PAGE/immunoblotting (*top*). Quantitation of ESRRB protein in CHX assay normalized to endogenous β-actin expression (*bottom*). (**b**) Representative images of HEI-CO1 cells overexpressed with wild-type and Arg382Cys mutant ESRRB. Immunofluorescent staining (IFS) with anti-myc (green) antibody, and nuclei were counterstained with DAPI (blue). (Scale bars: 10 μm) (**c**) The same as in (**b**) except that the distribution of ESRRB in both the nuclear and cytoplasmic compartments was ascertained through subcellular fractionation, followed by analysis via SDS-PAGE and immunoblotting (*left*). The resulting data were then quantified and plotted (*right*) as mean ± SEM (n = 3), *n.s.* no significance, $p > 0.05$. (**d**) The SMAD7 promoter-driven luciferase reporter and the ESRRB wild-type and Arg382Cys mutant construct were introduced into HEI-OC1 cells. Relative luciferase activity (wild-type as control) was plotted as mean ± SEM (n = 3), $^{**}p < 0.01$; $^{***}p < 0.001$, one-way ANOVA followed by Bonferroni's multiple comparison test.

missense variant (c.1144C>T; p.(Arg382Cys)) *in trans* with the canonical splicing variant (c.397 + 2T>G; p.?), we observed marked decreases in mRNA levels of *ATP1B1* and *EGR1* (decreased 55.1% and 45.4% respectively) in comparison with those in the father (SH635-1403: c.397 + 2T>G; p.?) (Fig. 5a). Similarly, mRNA levels of *ATP1B1* and *EGR1* decreased by 57.5% and 50.1%, respectively, in the mother. These results indicate that the *ESRRB* missense variant (p.Arg382Cys) could potentially exhibit pathogenicity by regulating downstream target gene expression essential for inner ear function.

In addition, we observed a significant reduction in the *ESRRB* mRNA level that in both the proband (SH635-1252) and the father (SH635-1403) compared to that in the mother (SH635-1402) (Fig. 5b). The c.397 + 2T>G splicing event was found to induce exon 4 skipping, leading to the formation of a premature stop codon followed

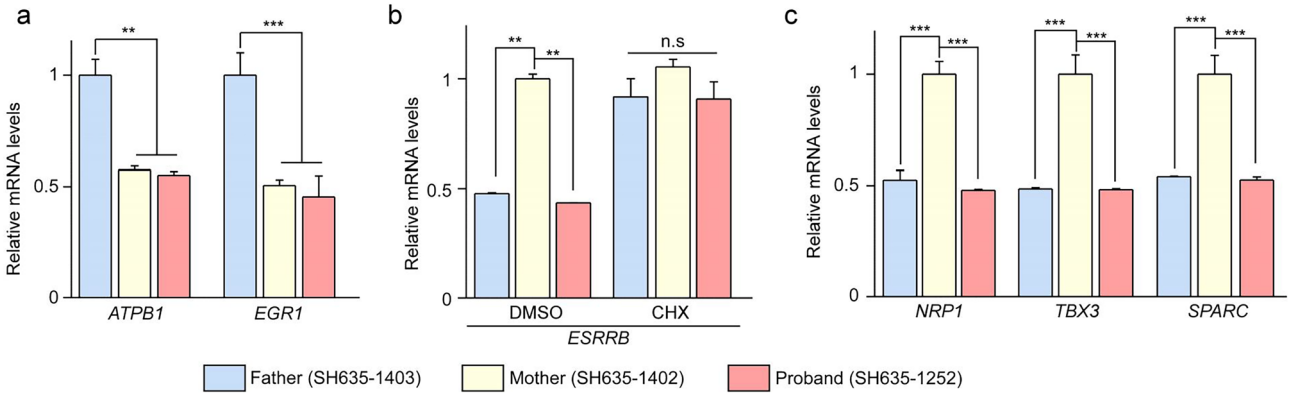

Fig. 5. Change in expression of *ESRRB* target genes. (**a**) Total RNA was isolated from father and proband derived lymphoblastoid cell lines (LCLs) and target genes (*ATP1B1* and *EGR1*) of *ESRRB* were analyzed by qRT-PCR. *GUSB* mRNA levels were used to normalize expression results. Values are presented as mean ± SEM of three independent experiments (N = 3); $^{**}p < 0.01$, $^{***}p < 0.001$ (n = 3, one-way ANOVA with Bonferroni's multiple comparison test). (**b**) Patient-derived LCLs were treated with DMSO or CHX (50 µg/mL) for 6 h, and the levels of ESRRB transcripts were confirmed. Quantitative reverse transcription polymerase chain reaction (qRT-PCR) analyses were conducted, targeting *ESRRB*. *GUSB* mRNA levels were used for normalization of *ESRRB* expression. Each bar represents means of percent values (relative to *ESRRB* mRNA level in wild-type fibroblast cells) ± SEM from three independent experiments (n.s., not significant, $^{**}p < 0.01$ one-way ANOVA with Bonferroni post hoc test). (**c**) The same as in (**a**) except that total RNA was extracted from LCLs obtained from the mother and the proband. Subsequently, expression levels of target genes *NRP1*, *TBX3*, and *SPARC* were examined using qRT-PCR. $^{***}p < 0.001$ (n = 3, one-way analysis of variance (ANOVA) followed by Bonferroni's multiple comparison test).

by NMD. To verify this, cells were treated with cycloheximide (CHX), a well-established inhibitor of NMD. The treatment resulted in the stabilization of *ESRRB* mRNA, suggesting that the reduction in *ESRRB* mRNA is dependent on the NMD pathway (Fig. 5b). In subsequent analyses, the *ESRRB* c.397 + 2T>G variant was associated with notable reductions of downstream target gene expression levels in the proband compared with the mother, including *NRP1*, *TBX3*, and *SPARC* (Fig. 5c) with reductions of 47.9%, 48.2%, and 52.6%, respectively, compared to those in the mother. Similarly, mRNA levels of *NRP1*, *TBX3*, and *SPARC* decreased by 52.4%, 48.5%, and 54.1% respectively, in the father.

Literature review and genotype–phenotype correlation

To date, 25 variant alleles of *ESRRB* (condensed to 22 when considering the same variants) have been reported to cause *ESRRB*-associated DFNB35, including variants found in the present study. The mutational spectrum included 20 (90.9%) single nucleotide variants, 1 (4.5%) indel, and 1 (4.5%) duplication. They could be further categorized into 16 (72.7%) missense variants, 1 (4.5%) nonsense variant, 2 (9.1%) frameshift variants, 2 (9.1%) splicing variants, and 1 (4.5%) in-frame variant. Of the 19 coding variants, all were located in functional domains except for one variant (c.16A>G:p.Arg6Gly). Nine were resided in the LBD while the remaining 9 were positioned in the DNA binding domain (DBD). In all affected DFNB35 patients, the type of hearing loss was identified as SNHL. Regardless of the two functional domains, no significant differences were noted in clinical phenotypes of hearing loss (onset, severity, and symmetry), precluding a clear genotype–phenotype correlation. The majority of hearing loss phenotypes exhibited symmetry, prelingual onset, and severe-to-profound SNHL, whereas our proband showed asymmetric hearing loss with a progressive nature. Although *ESRRB* disease-causing variants are found across various ethnic groups, a predominant occurrence is limited in consanguineous Pakistani families. This study represents the first documentation of *ESRRB*-related DFNB35 in South Korea. Consequently, the majority of reported cases exhibited homozygous zygosity except the p.(Arg382Cys) variant, which presented as a compound heterozygous variant in trans with either c.16A>G in a Han Chinese family or c.397 + 2T>G in a South Korean family.

Discussion

We, for the first time, report *ESRRB*-related DFNB35 in South Korea specifically harboring a novel splicing variant (NM_004452.4(ESRRB): c.397 + 2T>G) *in trans* with a missense variant (NM_004452.4(ESRRB): c.1144C>T p.(Arg382Cys)). While the pathogenicity of the splicing variant (c.397 + 2T>G: p.?) which causes exon skipping and consequent NMD is clear, the pathogenicity of the missense variant (p.(Arg382Cys) remains questionable despite its recurrent characteristics documented with *ESRRB*-related DFNB35 in the literature. Molecular modeling and dynamics studies have demonstrated that the p.(Arg382Cys) variant can significantly disrupt intramolecular interactions in LBD and conformational changes in the ESRRB protein. Biochemical assays corroborated these findings, showing reduced transcriptional activity and altered expression of downstream target genes essential for inner ear function. The current study expanded the genotypic spectrum of *ESRRB* in DFNB35 and refined molecular mechanisms underlying *ESRRB*-associated DFNB35. We suggest

that p.(Arg382Cys) variant can possess the functional pathogenicity despite a high allele frequency, thereby justifying its reclassification as a 'warm VUS' with evidence of causality.

This structural insight evidenced in this study aligns with previous research indicating that the LBD's structural integrity is pivotal for ERR beta protein function[29]. Based on the crystal structure of ESRRB models, we pointed to the critical role of the Glu337-Arg382 interaction (e.g., salt bridge) in stabilizing this helical loop region of the protein. Furthermore, our investigation supports the importance of the helical linker region between α-helices 7 and 8 in the context of LBD's structure stability and transcriptional function[30]. Several disease-causing variants in the helical linker region between α-helices 7 and 8 (p.(Leu320Pro) in α-helix 7, p.(Val342Leu) in α-helix 8, and p.(Leu347Pro) in α-helix 8) have been documented. For example, the p.(Glu340del) variant can compromise the stability of α-helix 8 implicated in DFNB35, underscoring the importance of the helical linker region between α-helices 7 and 8 in LBD's structural and functional integrity. Little is known about α-helix 9, where the Arg382 residue is located. It does not appear to directly engage with ligands or coactivators. However, the p.(Arg382Cys) variant can severely disrupt key intramolecular interactions in LBD, including instabilities in α-helices 7 and 8. This regional instability in LBD therefore can influence overall conformational changes and instability, as demonstrated by stability assay and dynamics studies.

The functional pathogenicity of the p.(Arg382Cys) variant appears to be indisputable. First, luciferase reporter assays showed that the transcriptional activity of the mutant ESRRB was abolished compared to that of the wild-type protein. Previous studies have established a significant role of mouse Esrrb, a key component of the core transcriptional regulatory network, in mouse embryonic stem (ES) cells[31–33]. The reduced transcriptional activity could be primarily attributable to the compromised stability of the mutant protein. Second, the p.(Arg382Cys) variant can alter downstream target gene expression, which is crucial for inner ear function. Given the spatiotemporal expression of ESRRB during inner ear development and its expression in the cochlea postnatally[14], the observed reduction in downstream gene expression attributed to the novel splicing variant (c.397 + 2T>G:p.?) and the missense variant (c.1144C>T:p.(Arg382Cys)) could impair normal development and functionality of the inner ear. Specifically, the p.(Arg382Cys) variant was found to reduce the expression of genes such as *ATP1B1* crucial for encoding components of the sodium/potassium-transporting ATPase enzyme necessary for maintaining ion gradients in hair cells[23,24]. A decrease in *ATP1B1* expression may result in hearing loss. Moreover, *EGR1* that is active in neuronal growth and the auditory cortex can significantly contribute to auditory processing[27]. Its downregulation might impair hearing acuity. While this study focused on selective genes of interest, the marked reduction in inner-ear specific transcriptional activity due to the p.(Arg382Cys) variant might contribute to pathogenic mechanisms underlying *ESRRB*-associated DFNB35. Third, upon elucidating functional pathogenicity of the p.(Arg382Cys) variant, we obtained additional evidence of PS3_supporting, permitting the reclassification as a 'warm VUS' with evidence of causality. Indeed, according to the ACGS Best Practice Guidelines, it is stated that VUS should be reported only when there is substantial supporting evidence, such as 'hot/warm VUS' classifications.

With advancement of NGS technologies and bioinformatics, there is a gradual decrease of diagnostic odyssey and undiagnosed cases. Meanwhile, the prevalence of VUS, whose interpretation is subject to debate, is also rising. Evidence of clinical utility of functional assays and integration of multi-omics have increasingly caused revisits for the pathogenicity of VUS, leading to their reclassification to 'likely pathogenic' and enabling more rapid and accurate diagnoses, which can directly inform clinical management strategies[34]. For example, in prior studies conducted by our group, variants in transcription factors such as *POU4F3* (p.Leu248Pro, p.Phe293Leu, and p.Val318Met) and *LMX1A* (p.Gln240Arg) were initially categorized as VUS under the ACMG/AMP guidelines[35,36]. Subsequent functional assays, which verified reduced activities of these transcription factors and changes transcriptome profiles associated with inner ear development, allowed us to confirm their pathogenicity. Upon criteria for classifying pathogenicity of variants, the PS3 criterion requires comprehensive functional assays such as gene or mRNA analysis to demonstrate a gene's deleterious effect[20,21]. The credibility of these assays is enhanced through methods involving replication, diverse methodologies pertinent to molecular mechanisms, and stringent control measures. Addition of PS3_supporting criteria is acknowledged when the assay is rigorously validated, encompassing comprehensive positive and negative controls, and when results consistently correspond to known functionalities of proteins involved[20]. For *GJB2*, methods like electrical or dye diffusion are employed to evaluate the activity of gap junction channel, while *SLC26A4* analysis often involves radioactive or fluorescent techniques to estimate the performance of anion exchanger and membrane trafficking. Through an in-depth comparative analysis of the *ESRRB* p.(Arg382Cys) variant in this study, assessing its transcription factor role using qRT-PCR and reporter gene assay, and evaluating protein stability against both normal and variant controls through immunoblotting in replicated manner, encompassing inner ear-specific cells, we could justify its categorization as PS3_supporting and its reclassification as a 'warm VUS' with evidence of causality. These insights derived from functional studies have potential to provide a breakthrough for cases where VUS, a previously unexplored variant, could be reinterpreted by elucidating its functional roles and disease-causing characteristics, potentially guiding natural course of disease phenotypes and clinical implications.

In scenarios where variants with high allele frequency demonstrate pathogenicity, key considerations include mutational hotspots and likelihood of a founder variant in specific ethnicity. Notable examples are *USH2A* c.2802T>G:p.(Cys934Trp) and c.8559-2A>G variants identified as East Asian-specific mutational hotspots implicated in retinitis pigmentosa or Usher syndrome type II[37]. The high allele frequency of the *ESRRB* p.(Arg382Cys) variant particularly in Korean and East Asian populations, while this variant is almost undetectable in other ethnicities, suggests the potential of an East Asian-specific mutational hotspot. Another aspect to consider is the incomplete penetrance. Similarly, the prevalence of Gitelman syndrome is likely underestimated due to its incomplete penetrance or late-onset progressive nature, which is associated with common variants in the *SLC12A3* with functional pathogenicity (e.g., p.Thr180Lys)[38]. An illustrative example is the *GJB2* c.109G>A(p.Val37Ile) variant classified as a hypomorphic allele[39], leading to a milder phenotype than other variants even

or manifesting incomplete penetrance. In this sense, the *ESRRB* p.(Arg382Cys) variant could be a hypomorph variant that can only lead to a disease phenotype when it is combined with a loss-of-function allele *in trans*. The hypomorphic variants or those with incomplete penetrance, including the *ESRRB* p.(Arg382Cys) variant, are less likely to undergo natural selection, which can lead to an increased carrier frequency.

In summary, our findings expanded the genotypic spectrum of *ESRRB* in DFNB35. This study investigated functional effects of *ESRRB*, an overlooked p.(Arg382Cys) variant, based on molecular modeling and dynamics, as well as diverse biochemical assays. Through this, we can uplift the classification of *ESRRB* p.(Arg382Cys) variant as 'warm VUS' with evidence of causality. Although more experimental evidences are required to uplift its pathogenic classification to 'likely pathogenic' or 'pathogenic', we suggest the probability that it is a functional variant with pathogenic potential. Further researches using *ESRRB* knock-in mouse are valid to confirm the pathogenicity of the p.(Arg382Cys) variant. This breakthrough extends our current understanding of SNHL genetics, arguing against the notion that a high allele frequency is inversely correlated to pathogenic potential and highlighting the importance of performing functional characterization of yet-to-be-explored VUS linked to clinical phenotypes.

Methods

Participants

This study utilized a retrospective design and focused on participants attending the Hereditary Hearing Loss Clinic within the Otorhinolaryngology division at the Center for Rare Diseases, Seoul National University Hospital, Korea, from 2021 March to 2023 December. One Korean family (SNUH635) with *ESRRB* compound heterozygous variants was included in the analysis. The demographics and clinical phenotypes of the proband were retrieved from the electronic medical records. The multidisciplinary molecular board meetings were conducted comprising clinicians and genome scientists and determined the pathogenicity of *ESRRB* variants. All procedures were approved by the Institutional Review Board of Seoul National University Hospital (no. IRB-H-0905–041-281).

Whole exome sequencing

Genomic DNA was extracted from peripheral blood using the Chemagic 360 instrument (Perkin Elmer, Baesweiler, Germany) and was subjected to WES using a SureSelect 50 Mb Hybridization and Capture Kit (Agilent Technologies, Santa Clara, CA, USA). The library was paired-end sequenced in compliance with the instructions provided by the manufacturer and using an Illumina NovaSeq 6000 sequencing system (Illumina, San Diego, CA, USA). The GRCh37 (hg19) was used as the reference sequence for mapping and variant calling, and we implemented the Genome Analysis Toolkit (GATK) optimal pipeline to call for single nucleotide variations (SNVs) and indels[40]. We applied the ANNOVAR software for variant annotation. As previously described[9,35,41], bioinformatics analysis and strict filtering were performed to retrieve candidate variants of hearing loss. (i) Non-synonymous variants with quality scores > 30 and read depths > 10 were selected (ii) Each variants with minor allele frequencies (MAFs) ≤ 0.001 were chosen based on population database, including gnomAD (https://gnomad.broadinstitute.org/), and ethnically-matched controls (Korean Reference Genome Database (KRGDB), http://152.99.75.168:9090/KRGDB/welcome.jsp) and KOVA2 databases (https://www.kobic.re.kr/kova/search_detail_view_hg19). (iii) The pathogenic potential of each variant was determined using in-silico tools CADD, https://cadd.gs.washington.edu/ and REVEL, https://sites.google.com/site/revelgenomics/), and SpliceAI (https://spliceailookup.broadinstitute.org/). In addition, we used the GERP + + score from the UCSC Genome Browser (http://genome.ucsc.edu/) to estimate the evolutionary conservation of the amino acid sequences. (iv) Furthermore, compatibility with inheritance patterns and audiological/clinical phenotypes was evaluated. Additionally, the ClinVar and HGMD databases were screened to check whether candidate variants had been previously identified in other patients. (v) The candidate variants were confirmed through Sanger sequencing, and a segregation study was performed using parental DNA samples. In addition, in accordance with methodologies outlined in previous studies[42,43], we applied two NGS-based CNV detection algorithms. We implemented CNVkit[44] and CoNIFER[45], which were used for the systematic screening of CNVs. In addition, copy number changes of candidate regions resulting from the CNV detection algorithms were inspected visually and confirmed using IGV. Resultantly, we classified the pathogenicity of candidate variants according to the ACMG-AMP guidelines for hearing loss, including pathogenic, likely pathogenic, VUS, likely benign, and benign[20]. We also classified the VUS using UK Association for Clinical Genomic Science Practice Guidelines, including hot, warm, tepid and cool[21].

Molecular modeling and molecular dynamics simulation

The crystal structure of the wild-type ESRRB protein was obtained from the Protein Data Bank (PDB IDs: 6LN4 and 6LIT). The mutant model was generated using PyMOL software (ver. 2.5.2). The structural model obtained in the previous process was identify those residues which have bad torsion angles, or VanderWaals' clashes, or total energy, and repairs them using Foldx 5 software. Intramolecular interactions, including hydrophobic interactions, hydrogen bonds, and salt bridges, were compared to predict the effects of *ESRRB* variants on regional protein stability. All graphical illustrations were produced using PyMOL software (ver. 2.5.2) (PyMOL Molecular Graphics System ver. 2.0, Schrödinger Inc., New York, NY, USA). Furthermore, GROMACS 2023.1 was utilized to evaluate the impact of the identified variant on protein stability and function[46]. The p.(Arg382Cys) variant was evaluated in a computationally simulated environment to determine its influence on protein stability and function. Specifically, a molecular dynamics simulation of the p.(Arg382Cys) variant was performed using GROMACS 2023.1 with the OPLS force field (OPLS-AA/L all-atom force field, 2001 aminoacid dihedrals); the PBC box type was cubic and centers the protein in the box and places it at least 1.0 nm from the box edge. The

SPC216 water model was employed, which is a generic equilibrated 3-point solvent model, and the system was neutralized by replacing a solvent molecule with NA + ions. Comparative analyses of the structural deviation in the wild-type and mutant (p.Arg382Cys) structures were computed using GROMACS-associated utility packages such as g_rms, g_rmsf, g_gyrate, and g_sasa. All graphs were plotted using GRACE software (ver.5.1.25 http://plasma-gate.weizmann.ac.il/Grace/).

In vitro splicing analysis using minigene assay

To investigate the effect of the novel splicing variant (c.397 + 2T>G:p.?), in vitro analysis was carried out utilizing the pSPL3 exon trapping vector, following the procedure as previously described[47,48]. Briefly, exon 4 of the *ESRRB* gene, flanked by an upstream intron and a downstream intronic sequence containing both wild-type and mutant alleles, was amplified using specific primers that introduced EcoRI and NdeI restriction sites. After cloning the amplified product into the pSPL3 vector, direct sequencing confirmed that all constructs possess the correct sequence. The constructs were individually transfected into HEK293T cells. The cells were cultured in a humidified incubator with 5% CO_2 at 37 °C, using DMEM supplemented with 10% FBS, 2 mM glutamine, and 100 units/mL penicillin/streptomycin. Regular mycoplasma tests were conducted to ensure their quality. Cells were transfected with 2 µg of plasmid DNA in a 6-well culture plate (> 70% confluent) for 24 h using Lipofectamine 3000 (Invitrogen), following the manufacturer's guidelines. Total RNA from cultured cells was extracted using the TRIzol Reagent (Invitrogen). To ensure RNA purity and eliminate any contaminating DNA, on-column DNase I treatment was carried out using RNeasy Mini-Columns (Qiagen). cDNA samples were prepared by reverse transcription using the Accupower RT-preMix (Bioneer). Subsequently, PCR was conducted using diluted cDNA and 10 pmol of vector-specific primers to assess the in vitro splicing efficiency. The vector-specific primer sequences were as follows: a forward primer SD6 (5′-TCTGAGTCACCTGGACAACC-3′) and a reverse primer SA2 (5′- ATCTCAGTGGTATTTGTGAGC-3′). The thermal cycling conditions consisted of an initial denaturation at 95 °C for 5 min, followed by 34 cycles of 95 °C for 30 s, 60 °C for 30 s, and 72 °C for 1 min. The amplified DNA was visualized using agarose gel electrophoresis with Loading STAR (DYNE Bio) and gene transcripts were analyzed by Sanger sequencing using vector-specific primers.

Lymphoblastoid cell culture and quantitative real-time PCR (qRT-PCR)

LCLs were established using standard procedures by transforming fresh lymphocytes from the SNUH 635 family with the Epstein-Barr Virus (EBV)[49]. LCLs were cultured at 37 °C in a 5% CO_2 atmosphere using RPMI-1640 medium supplemented with 20% FBS and antibiotics (100 units/mL penicillin/streptomycin). LCLs were initially seeded at 4×10^5 cells/ml and harvested after 4 days for RNA isolation. Total RNA was extracted from 5×10^6 cell pellets using the TRIzol Reagent, followed by additional purification using RNeasy mini-columns. To prepare cDNA samples, two micrograms of total RNA were subjected to reverse transcription. For the quantitative RT-PCR reactions, 1/20 diluted cDNA was utilized as the template, together with SYBR qPCR master mixture (Enzynomics) as the reporter dye, and 10 pmol of gene-specific primers were employed to detect the mRNA expression of specific genes. The thermal cycling conditions consisted of an initial denaturation and enzyme activation step at 95 °C for 10 min, followed by 40 cycles of amplification at 95 °C for 15 s, 60 °C for 20 s, and 72 °C for 15 s. The mRNA levels of each target gene were normalized to the GUSB (glucuronidase beta) levels of each cDNA sample[50]. The experimental results were expressed as the relative fold values, presented as the mean ± standard deviation (SD) from three independent experiments. The primer sequences used for amplifying the target genes were as follows: for *ESRRB*, forward (5′- TCGCTGCCCTATGACGACA -3′) and reverse (5′- CTT CTTGTACCTGCGTACCAG -3′); for *SPARC*, a forward primer (5′- CCCATTGGCGAGTTTGAGAAG-3′) and a reverse primer (5′- CAAGGCCCGATGTAGTCCA-3′); for *TBX3*, forward (5′- CCCGGTTCCACATTGTAA GAG-3′) and reverse (5′- GTATGCAGTCACAGCGATGAAT-3′); for *NRP1*, forward (5′- ACGTGGAAGTCT TCGATGGAG-3′) and reverse (5′- CACCATGTGTTTCGTAGTCAGA-3′); for *ATP1B1*, forward (5′- CCGGTG GCAGTTGGTTTAAGA-3′) and reverse (5′- GCATCACTTGGATGGTTCCGA-3′); for *EGR1*, forward (5′- GGT CAGTGGCCTAGTGAGC-3′) and a reverse (5′- GTGCCGCTGAGTAAATGGGA-3′); for *GUSB*, forward (5′- CACCAGGGACCATCCAATACC-3′) and reverse (5′- GCAGTCCAGCGTAGTTGAAAAA-3′).

Stability assay

In the cycloheximide chase assay, cells were first grown to 80% confluence and transfected with both the wild-type and the ESRRB mutant for 48 h. Subsequently, cells were treated with cycloheximide (80 µg/ml) to block new protein synthesis. At predetermined time points (0, 1, 2, 4, and 6 h post-treatment), cells were harvested and lysed for protein extraction. Equal amounts of protein were separated by SDS-PAGE, transferred to PVDF membranes, and probed with specific antibodies against the protein of interest and a housekeeping protein, specifically β-actin, as a loading control. The intensity of the protein bands was quantified using densitometry (Image J software ver. 1.54d, NIH) allowing for the assessment of protein degradation over time.

Subcellular fractionation

Cells were collected by centrifugation, washed with PBS and nuclear and cytosolic fractions were obtained using the Subcellular Protein Fractionation Kit (Cat#78840, Thermo Fisher Scientific), following the manufacturer's instructions. SP1 and Calnexin antibodies were used as markers for nuclear and cytosolic fractions, respectively.

Immunocytochemistry

For immunocytochemistry, HEK293T and HEI-OC1 cells were seeded on coverslip, transiently overexpressed with both wild-type and mutant ESRRB for 48 h. Subsequently, cells were fixed with 4% paraformaldehyde in PBS for 20 min. After that, the fixed cells were permeabilized with 0.5% (v/v) Triton X-100 in PBS for 10 min, blocked

with 2% BSA in PBS, and incubated with primary antibodies such as anti-Myc antibody (1:100 dilution) in the blocking solution for 15 h in 4 °C. After several washing steps, the cells were incubated for 40 min with Alexa Fluor 488–conjugated secondary antibodies diluted (1:1,000) for additional 1 h. The cells were then mounted with a 4′,6′-diamidino-2-phenylindole (DAPI)-containing mounting solution (Abcam). Most of the fluorescent signals were monitored and captured using an confocal confocal microscope STELLARIS 8 (Leica). All images were taken with the same microscope settings, ensuring consistency and accurately representing the entire cell population.

Expression plasmid and luciferase reporter assay

An ESRRB Human Tagged ORF clone, specifically the pCMV6-ESRRB wild-type-Myc-DDK (RC215995), was acquired from Origene. This ESRRB plasmid underwent modification through site-directed mutagenesis to create the pCMV6-ESRRB p.(Arg382Cys) variant. The plasmids, including the pCMV6-Myc-DDK entry vector, were introduced into the DH5α bacterial strain for the purpose of isolating recombinant plasmids, which were later confirmed via DNA sequencing. The extracted plasmid DNA was then purified and concentrated using the plasmid maxi kit (A2392, Promega) as per the provided instructions, and subsequently stored at a temperature of − 20 °C for future use. In the case of the 293 T cell line, cells were cultured in an environment with 5% CO2 at 37 °C, ensuring a humid atmosphere. To achieve transient overexpression, these cells were transfected with 1–2 μg of the total plasmid DNA per well in a 6-well culture plate, ensuring at least 80% cell confluence. This process was conducted over a 24-h period using the Lipofectamine 3000 reagent (L3000015, Invitrogen), following the manufacturer's protocol. For the luciferase assay, as previously described[51,52], the pGL4.12[luc2CP]-SMAD7 construct, containing a luciferase reporter, was employed. This assay was performed according to the manufacturer's instructions (E1500, Promega). Briefly, HEK293T cells transfected with pGL4.12[luc2CP]-SMAD7, pCMV6-ESRRB p.(Arg382Cys), and pCMV6-ESRRB wild-type constructs were lysed. Then, 20 μl of the resultant cell lysate was combined with 100 μl of Luciferase Assay Reagent. The light emitted was measured using the Synergy Mx Microplate Reader (BioTek). The luciferase activity, a marker of transcriptional activity, for both the wild-type and ESRRB mutant, was standardized against an internal control, which in this case was the Myc-DDK-transfected empty vector.

Ethics declarations

Ethical approval and informed consent were obtained for the participation of one Korean family (SNUH635) with ESRRB compound heterozygous variants in the analysis. All procedures were approved by the Institutional Review Board of Seoul National University Hospital (no. IRB-H-0905-041-281). The National Institutes of Health Guide for the Care adhered to during the implementation of all experimental protocols.

Data availability

All data generated or analyzed during this study are included in this published article and its supplementary information files. The crystallographic structure of ESRRB utilized in this investigation was acquired from Protein Data Bank (PDB IDs: 6LN4 and 6LIT). All data are available from the corresponding author upon reasonable request. Supplementary information includes uncropped western blots for each figure.

Received: 24 January 2024; Accepted: 21 August 2024
Published online: 11 September 2024

References

1. Petit, C., Bonnet, C. & Safieddine, S. Deafness: From genetic architecture to gene therapy. *Nat. Rev. Genet.* **24**, 665–686. https://doi.org/10.1038/s41576-023-00597-7 (2023).
2. Bowl, M. R. *et al.* A large scale hearing loss screen reveals an extensive unexplored genetic landscape for auditory dysfunction. *Nat. Commun.* **8**, 886. https://doi.org/10.1038/s41467-017-00595-4 (2017).
3. Liao, E. N., Taketa, E., Mohamad, N. I. & Chan, D. K. Outcomes of gene panel testing for sensorineural hearing loss in a diverse patient cohort. *JAMA Netw. Open* **5**, e2233441. https://doi.org/10.1001/jamanetworkopen.2022.33441 (2022).
4. Downie, L. *et al.* Exome sequencing in infants with congenital hearing impairment: A population-based cohort study. *Eur. J. Hum. Genet.* **28**, 587–596. https://doi.org/10.1038/s41431-019-0553-8 (2020).
5. Gu, X. *et al.* Genetic testing for sporadic hearing loss using targeted massively parallel sequencing identifies 10 novel mutations. *Clin. Genet.* **87**, 588–593. https://doi.org/10.1111/cge.12431 (2015).
6. Jung, J. *et al.* Genetic predisposition to sporadic congenital hearing loss in a pediatric population. *Sci. Rep.* **7**, 45973. https://doi.org/10.1038/srep45973 (2017).
7. Nakanishi, H. *et al.* NLRP3 mutation and cochlear autoinflammation cause syndromic and nonsyndromic hearing loss DFNA34 responsive to anakinra therapy. *Proc. Natl. Acad. Sci. U S A* **114**, E7766–E7775. https://doi.org/10.1073/pnas.1702946114 (2017).
8. Jiang, L., Wang, D., He, Y. & Shu, Y. Advances in gene therapy hold promise for treating hereditary hearing loss. *Mol. Ther.* **31**, 934–950. https://doi.org/10.1016/j.ymthe.2023.02.001 (2023).
9. Nam, D. W. *et al.* Allelic hierarchy for USH2A influences auditory and visual phenotypes in South Korean patients. *Sci. Rep.* **13**, 20239. https://doi.org/10.1038/s41598-023-47166-w (2023).
10. Carlson, R. J. *et al.* Association of genetic diagnoses for childhood-onset hearing loss with cochlear implant outcomes. *JAMA Otolaryngol. Head Neck Surg.* **149**, 212–222. https://doi.org/10.1001/jamaoto.2022.4463 (2023).
11. Tabatabaei, Z., Farazi Fard, M. A., Hashemi, S. B. & Dianatpour, M. Identification of novel microsatellite markers flanking GJB2 gene in order to use in preimplantation genetic diagnosis of hearing loss: A comparison of whole-genome amplification and semi-nested PCR. *Eur. J. Med. Genet.* **63**, 103796. https://doi.org/10.1016/j.ejmg.2019.103796 (2020).
12. Wright, C. F., FitzPatrick, D. R. & Firth, H. V. Paediatric genomics: Diagnosing rare disease in children. *Nat. Rev. Genet.* **19**, 253–268. https://doi.org/10.1038/nrg.2017.116 (2018).
13. Chiereghin, C. *et al.* SLC22A4 gene in hereditary non-syndromic hearing loss: Recurrence and incomplete penetrance of the p.C113Y mutation in Northwest Africa. *Front. Genet.* **12**, 606630. https://doi.org/10.3389/fgene.2021.606630 (2021).

14. Collin, R. W. *et al.* Mutations of ESRRB encoding estrogen-related receptor beta cause autosomal-recessive nonsyndromic hearing impairment DFNB35. *Am. J. Hum. Genet.* **82**, 125–138. https://doi.org/10.1016/j.ajhg.2007.09.008 (2008).
15. Yao, B. *et al.* Structural insights into the specificity of ligand binding and coactivator assembly by estrogen-related receptor beta. *J. Mol. Biol.* **432**, 5460–5472. https://doi.org/10.1016/j.jmb.2020.08.007 (2020).
16. Uranishi, K., Akagi, T., Koide, H. & Yokota, T. Esrrb directly binds to Gata6 promoter and regulates its expression with Dax1 and Ncoa3. *Biochem. Biophys. Res. Commun.* **478**, 1720–1725. https://doi.org/10.1016/j.bbrc.2016.09.011 (2016).
17. Yang, T., Wei, X., Chai, Y., Li, L. & Wu, H. Genetic etiology study of the non-syndromic deafness in Chinese Hans by targeted next-generation sequencing. *Orphanet. J. Rare Dis.* **8**, 85. https://doi.org/10.1186/1750-1172-8-85 (2013).
18. Wu, C. C. *et al.* Identifying children with poor cochlear implantation outcomes using massively parallel sequencing. *Medicine* **94**, e1073. https://doi.org/10.1097/MD.0000000000001073 (2015).
19. Liu, Y. *et al.* Genetic profiles of non-syndromic severe-profound hearing loss in Chinese Hans by whole-exome sequencing. *Gene* **819**, 146258. https://doi.org/10.1016/j.gene.2022.146258 (2022).
20. Oza, A. M. *et al.* Expert specification of the ACMG/AMP variant interpretation guidelines for genetic hearing loss. *Hum. Mutat.* **39**, 1593–1613. https://doi.org/10.1002/humu.23630 (2018).
21. Sian Ellard, E. L. B., *et al. ACGS Best Practice Guidelines for Variant Classification in Rare Disease 2020*. https://www.acgs.uk.Com/media/11631/uk-practice-guidelines-for-variant-classification-v4-01-2020.pdf, Acessed 23 Dec 2023.
22. Alexandrovich, A. *et al.* Wnt2 is a direct downstream target of GATA6 during early cardiogenesis. *Mech. Dev.* **123**, 297–311. https://doi.org/10.1016/j.mod.2006.02.002 (2006).
23. Scheffer, D. I., Shen, J., Corey, D. P. & Chen, Z. Y. Gene expression by mouse inner ear hair cells during development. *J. Neurosci.* **35**, 6366–6380. https://doi.org/10.1523/JNEUROSCI.5126-14.2015 (2015).
24. Liu, W. & Rask-Andersen, H. Na/K-ATPase gene expression in the human cochlea: A study using mRNA in situ hybridization and super-resolution structured illumination microscopy. *Front. Mol. Neurosci.* **15**, 857216. https://doi.org/10.3389/fnmol.2022.857216 (2022).
25. Salehi, P. *et al.* Role of Neuropilin-1/Semaphorin-3A signaling in the functional and morphological integrity of the cochlea. *PLoS Genet.* **13**, e1007048. https://doi.org/10.1371/journal.pgen.1007048 (2017).
26. Mothe, A. J. & Brown, I. R. Expression of mRNA encoding extracellular matrix glycoproteins SPARC and SC1 is temporally and spatially regulated in the developing cochlea of the rat inner ear. *Hear Res.* **155**, 161–174. https://doi.org/10.1016/s0378-5955(01)00246-5 (2001).
27. Wang, M. *et al.* Characterization of EGR-1 expression in the auditory cortex following kanamycin-induced hearing loss in mice. *J. Mol. Neurosci.* **71**, 2260–2274. https://doi.org/10.1007/s12031-021-01791-0 (2021).
28. Kaiser, M. *et al.* Regulation of otocyst patterning by Tbx2 and Tbx3 is required for inner ear morphogenesis in the mouse. *Development* **148**, 195651. https://doi.org/10.1242/dev.195651 (2021).
29. Ghasemnejad, T., Shekari Khaniani, M., Nouri Nojadeh, J. & Mansoori Derakhshan, S. A novel missense variant in ESRRB gene causing autosomal recessive non-syndromic hearing loss: In silico analysis of a case. *BMC Med. Genom.* **15**, 18. https://doi.org/10.1186/s12920-022-01165-4 (2022).
30. Lee, K. *et al.* A novel ESRRB deletion is a rare cause of autosomal recessive nonsyndromic hearing impairment among Pakistani families. *Genet. Res. Int.* **2011**, 368915. https://doi.org/10.4061/2011/368915 (2011).
31. van den Berg, D. L. *et al.* Estrogen-related receptor beta interacts with Oct4 to positively regulate Nanog gene expression. *Mol. Cell Biol.* **28**, 5986–5995. https://doi.org/10.1128/MCB.00301-08 (2008).
32. Wang, J. *et al.* A protein interaction network for pluripotency of embryonic stem cells. *Nature* **444**, 364–368. https://doi.org/10.1038/nature05284 (2006).
33. Uranishi, K., Akagi, T., Sun, C., Koide, H. & Yokota, T. Dax1 associates with Esrrb and regulates its function in embryonic stem cells. *Mol. Cell Biol.* **33**, 2056–2066. https://doi.org/10.1128/MCB.01520-12 (2013).
34. Lunke, S. *et al.* Integrated multi-omics for rapid rare disease diagnosis on a national scale. *Nat. Med.* **29**, 1681–1691. https://doi.org/10.1038/s41591-023-02401-9 (2023).
35. Lee, S. Y. *et al.* Ramifications of POU4F3 variants associated with autosomal dominant hearing loss in various molecular aspects. *Sci. Rep.* **13**, 12584. https://doi.org/10.1038/s41598-023-38272-w (2023).
36. Lee, S. Y. *et al.* Novel molecular genetic etiology of asymmetric hearing loss: Autosomal-dominant LMX1A variants. *Ear Hear.* **43**, 1698–1707. https://doi.org/10.1097/AUD.0000000000001237 (2022).
37. Li, W. *et al.* Genetic characteristics and variation spectrum of USH2A-related retinitis pigmentosa and usher syndrome. *Front. Genet.* **13**, 900548. https://doi.org/10.3389/fgene.2022.900548 (2022).
38. Kondo, A. *et al.* Examination of the predicted prevalence of Gitelman syndrome by ethnicity based on genome databases. *Sci. Rep.* **11**, 16099. https://doi.org/10.1038/s41598-021-95521-6 (2021).
39. Chen, T. *et al.* Update of the spectrum of GJB2 mutations in 107 patients with nonsyndromic hearing loss in the Fujian population of China. *Ann. Hum. Genet.* **78**, 235–242. https://doi.org/10.1111/ahg.12062 (2014).
40. Van der Auwera, G. A. *et al.* From FastQ data to high confidence variant calls: The Genome Analysis Toolkit best practices pipeline. *Curr. Protoc. Bioinform.* **43**, 111011–111033. https://doi.org/10.1002/0471250953.bi1110s43 (2013).
41. Lee, S. Y. *et al.* Novel KCNQ4 variants in different functional domains confer genotype- and mechanism-based therapeutics in patients with nonsyndromic hearing loss. *Exp. Mol. Med.* **53**, 1192–1204. https://doi.org/10.1038/s12276-021-00653-4 (2021).
42. Cho, S. H. *et al.* Novel autosomal dominant TMC1 variants linked to hearing loss: Insight into protein-lipid interactions. *BMC Med. Genom.* **16**, 320. https://doi.org/10.1186/s12920-023-01766-7 (2023).
43. Yun, Y. *et al.* Expanding genotype-phenotype correlation of CLCNKA and CLCNKB variants linked to hearing loss. *Int. J. Mol. Sci.* **24**, 17077. https://doi.org/10.3390/ijms242317077 (2023).
44. Talevich, E., Shain, A. H., Botton, T. & Bastian, B. C. CNVkit: Genome-wide copy number detection and visualization from targeted DNA sequencing. *PLoS Comput. Biol.* **12**, e1004873. https://doi.org/10.1371/journal.pcbi.1004873 (2016).
45. Krumm, N. *et al.* Copy number variation detection and genotyping from exome sequence data. *Genome Res.* **22**, 1525–1532. https://doi.org/10.1101/gr.138115.112 (2012).
46. Van Der Spoel, D. *et al.* GROMACS: Fast, flexible, and free. *J. Comput. Chem.* **26**, 1701–1718. https://doi.org/10.1002/jcc.20291 (2005).
47. Wang, X. *et al.* Two Novel HOGA1 splicing mutations identified in a chinese patient with primary hyperoxaluria type 3. *Am. J. Nephrol.* **42**, 78–84. https://doi.org/10.1159/000439232 (2015).
48. Jonsson, F. *et al.* ATP-binding cassette subfamily A, member 4 intronic variants c.4773+3A>G and c.5461–10T>C cause Stargardt disease due to defective splicing. *Acta Ophthalmol.* **96**, 737–743. https://doi.org/10.1111/aos.13676 (2018).
49. Neitzel, H. A routine method for the establishment of permanent growing lymphoblastoid cell lines. *Hum. Genet.* **73**, 320–326. https://doi.org/10.1007/BF00279094 (1986).
50. de Brouwer, A. P., van Bokhoven, H. & Kremer, H. Comparison of 12 reference genes for normalization of gene expression levels in Epstein-Barr virus-transformed lymphoblastoid cell lines and fibroblasts. *Mol. Diagn. Ther.* **10**, 197–204. https://doi.org/10.1007/BF03256458 (2006).
51. Li, Q. S. & Zheng, P. S. ESRRB inhibits the TGFbeta signaling pathway to drive cell proliferation in cervical cancer. *Cancer Res.* **83**, 3095–3114. https://doi.org/10.1158/0008-5472.CAN-23-0067 (2023).

52. Lee, S. *et al.* Phenotypic and molecular basis of SIX1 variants linked to non-syndromic deafness and atypical branchio-otic syndrome in South Korea. *Sci. Rep.* **13**, 11776. https://doi.org/10.1038/s41598-023-38909-w (2023).

Author contributions

WHC and JHC performed in vitro experiments. YC, SHJ, SYL analyzed genetic data. JGJ, DHL and SYL performed the structural analysis. JJS and JHL provided the materials. WHC and SYL designed experiments and writing the manuscript. All authors read and approved the final manuscript.

Funding

This research was supported and funded by SNUH Kun-hee Lee Child Cancer & Rare Disease Project, Republic of Korea (FP-2022-00001-004 to S.-Y.L.), National Research Foundation of Korea (NRF) and funded by the Ministry of Education (grant number: 2022R1C1C1003147 to S.-Y.L.), SNU Medicine grant (basic and clinic cooperation research grant No. 800-20230428 to S.-Y.L), SNUH Research Fund (04-2022-4010 to S.-Y.L. and 04-2022-3070 to S.-Y.L.).

Competing interests

The authors declare no competing interests.

Additional information

Supplementary Information The online version contains supplementary material available at https://doi.org/10.1038/s41598-024-70795-8.

Correspondence and requests for materials should be addressed to S.-Y.L.

Reprints and permissions information is available at www.nature.com/reprints.

Publisher's note Springer Nature remains neutral with regard to jurisdictional claims in published maps and institutional affiliations.